catalysts

MDPI

Article

The Organic Bromide Sources Adjusting the Shape and Band Structures of BiOBr Nanosheets for Enhanced Photodegradation Performances of BPA

Donghao Xia, Kaiyang Sun, Youwei Zeng, Lulu Wang, Yi Zhang, Jie Shen *, Zhaohui Wu * and Wenhui Feng *

Hunan Key Laboratory of Applied Environmental Photocatalysis, Changsha University, Changsha 410022, China; xdh910672740@163.com (D.X.); s19163323744@163.com (K.S.); zyw210970@163.com (Y.Z.); wll_13928@163.com (L.W.); zhangyi2000521@163.com (Y.Z.)

* Correspondence: calfensj@gmail.com (J.S.); hubeiwzh1624@126.com (Z.W.); fengwenhui1991@126.com (W.F.); Tel.: +86-731-84261421 (J.S.)

Abstract: Bismuth oxybromide (BiOBr) nanosheets were prepared by employing organic bromide sources. In the presence of organic bromide sources, the effects of different conditions on the band structure, shape, size, and light responses of BiOBr nanosheets were examined. The reaction conditions, including different types of organic bromide sources, solvent, concentration, temperature, and time, were examined regarding the formation of BiOBr nanosheets. Then, the photocatalytic performances of different BiOBr nanosheets were also examined. Especially, the BiOBr nanosheets obtained from the addition of over 2 mmol of tetramethyl ammonium bromide (TMAB) in mannitol or EG at a higher temperature and longer reaction time showed superior photocatalytic activity. The enhanced photocatalytic performance of bisphenol A over these BiOBr nanosheets was achieved within 50 min due to efficient charge transfer and separation.

Keywords: organic bromide sources; shape; BiOBr nanosheets; photocatalytic performances

Citation: Xia, D.; Sun, K.; Zeng, Y.; Wang, L.; Zhang, Y.; Shen, J.; Wu, Z.; Feng, W. The Organic Bromide Sources Adjusting the Shape and Band Structures of BiOBr Nanosheets for Enhanced Photodegradation Performances of BPA. *Catalysts* **2022**, *12*, 820. https://doi.org/10.3390/catal12080820

Academic Editors: Amr Fouda and Mohammed F. Hamza

Received: 13 May 2022
Accepted: 28 June 2022
Published: 26 July 2022

Table S1. All the reactants and reaction conditions in this study.

No.	Solvent	$Bi(NO_3)_3 \bullet 5H_2O$ (mmol)	Bromide sources		Temp. (°C)	Time (h)	Abbreviation
			Types	Concen. (mmol)			
1	H_2O	2	KBr	2	180	4	KBr
2	H_2O	2	TMAB	2	180	4	TMAB, H_2O
3	H_2O	2	TBAB	2	180	4	TBAB
4	H_2O	2	CTAB	2	180	4	CTAB
5	Mannitol (0.02 M)	2	TMAB	2	180	4	Mannitol (0.02 M), 2 mmol, 180 °C, 4 h
6	EG	2	TMAB	2	180	4	EG
7	G	2	TMAB	2	180	4	G
8	Mannitol (0.02 M)	2	TMAB	2	120	4	120 °C
9	Mannitol (0.02 M)	2	TMAB	2	140	4	140 °C
10	Mannitol (0.02 M)	2	TMAB	2	160	4	160 °C
11	Mannitol (0.02 M)	2	TMAB	2	180	2	2 h
12	Mannitol (0.02 M)	2	TMAB	2	180	8	8 h
13	Mannitol (0.02 M)	2	TMAB	2	180	12	12 h
14	Mannitol (0.02 M)	1	TMAB	1	180	4	1 mmol
15	Mannitol (0.02 M)	4	TMAB	4	180	4	4 mmol

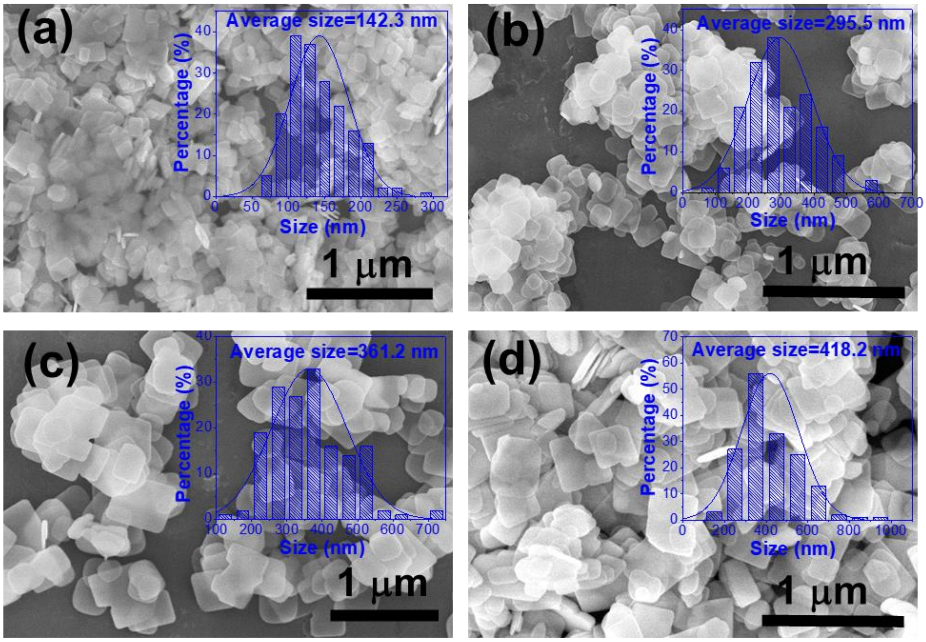

Figure S1. SEM images of samples prepared at different reaction time, (a) 2 h, (b) 4 h, (c) 8 h, (d) 12 h (inset with the corresponding average size of resulted samples).

As showed in Figure S1, all the resulted products were sheet-like morphology, but with different size and size distribution. Apparently, the size of generated BiOBr nanosheets were gradually increased from 142.3 nm to 418.2 nm when raising the reaction time. Based on previous reports, prolonging the reaction time, the Ostwald repining mechanism could drive the dissolution of small nanosheets for the local concentration increasing, which are contributed to the growth of larger nanosheets [1-3].

The Mott–Schottky plots of different samples obtained by adding different bromine sources were present in Figure S2. The flat band potentials of BiOBr nanosheets electrodes prepared by adding KBr was –1.39 eV (Ag/AgCl). While, the flat band potential values of BiOBr nanosheets electrodes obtained by adding TBAB and CTAB were similar, which were approached to –1.06 eV (Ag/AgCl), and the potential value was slightly increased to –1.0 eV for TMAB (Ag/AgCl). Then, the corresponding Fermi energies were –1.29 eV, –0.96 eV, and –0.9 eV (vs. NHE) for the BiOBr generated by adding KBr, TBAB (and CTAB), and TMAB, respectively [4, 5], which were closed to the value of conduction band.

Then, these values of conduction band were similar to the estimated values based on the VB-XPS (**Figure 6**).

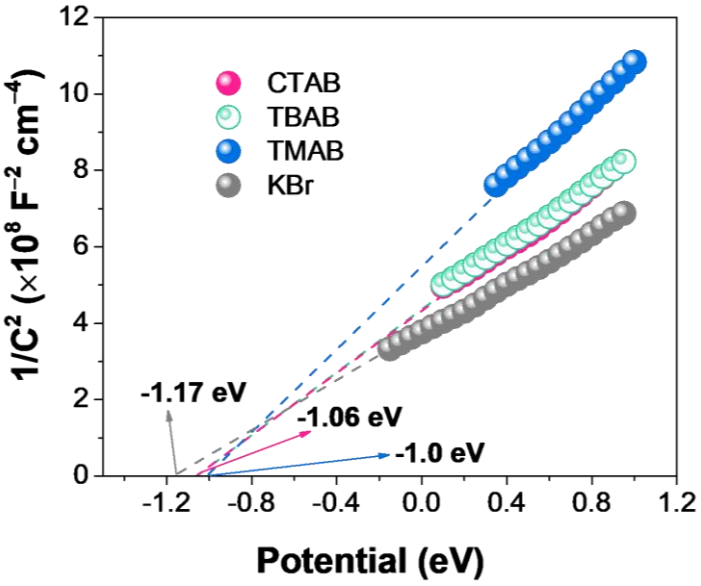

Figure S2. The Mott–Schottky plots of different samples electrodes at frequencies of 1000 Hz, versus the Ag/AgCl electrode.

The photocatalytic performances of other BiOBr nanosheets obtained at different conditions were also investigated (Figure S3). The BiOBr nanosheets with much smaller size exhibited superior photocatalytic performances that 70% of phenol were able to remove within 50 min irradiation due to the smaller size effect for efficient charge transfer and separation. While the photodegradation efficiency of BiOBr nanosheets obtained in mannitol and water were lower than that BiOBr nanosheets prepared in EG (**Figure S3a**). When prolonging the reaction time from 2 h to 12 h gradually, the photocatalytic performances of resulted BiOBr nanosheets were elevated correspondingly that BiOBr nanosheets obtained at 12 h showed relative higher photocatalytic activity owing to the enhanced crystallinity of resulted BiOBr nanosheets (**Figure S3b**). Similarly, the photocatalytic performance of BiOBr nanosheets obtained with the increasing temperature also showed increased trend that the relative higher photocatalytic performances were harvested over BiOBr nanosheets produced at 180 °C because of the increased crystallinity (**Figure S3c**).

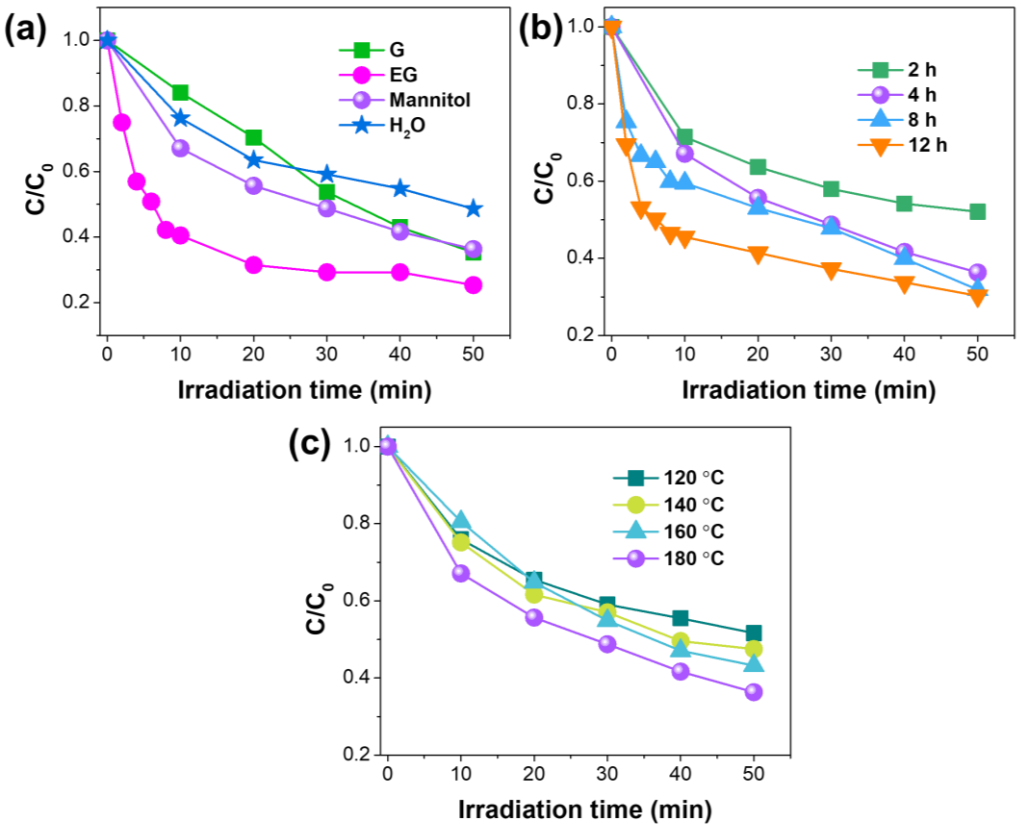

Figure S3. Photocatalytic performances of BiOBr nanosheets obtained at different conditions, (a) by adding different solvents, (b) at different reaction time, and (c) at different reaction temperature.

In the scavenger tests, the scavengers of isopropanol (IPA), triethanolamine (TEOA), ascorbic acid (AA), and for•OH, h^+, and $•O_2^-$, respectively. According to the results of scavenger tests (Figure S4), the photocatalytic activity was completely suppressed in the presence of AA, suggesting that the $•O_2^-$ is the predominant reactive species for photocatalysis. Comparatively, the photocatalytic performances were slightly hindered by adding TEOA, and the photocatalytic activities were scarcely affected, indicating that the h^+ is the minor active species and •OH can be ignored during the photocatalytic process.

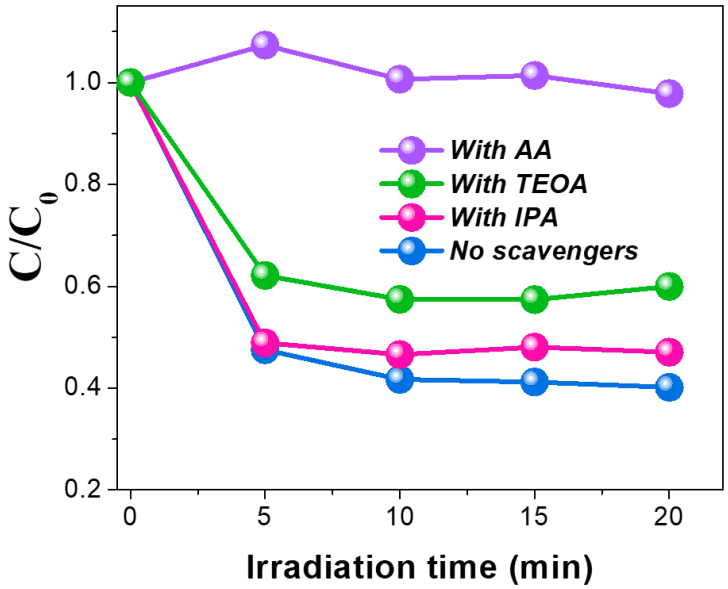

Figure S4. Scavenger tests of BiOBr nanosheets obtained in mannitol and in the presence of 2 mmol of TMAB, 180 °C, 4 h.

References

1. Zhang, C. W.; Xia, Y.; Zhang, Z. M.; Huang, Z.; Lian, L. Y.; Miao, X. S.; Zhang, D. L.; Beard, M. C. and Zhang, J. B., Combination of cation exchange and quantized Ostwald ripening for controlling size distribution of lead chalcogenide quantum dots, *Chem. Mater.* **2017**, 29, 3615–3622.
2. Houk, L. R.; Challa, S. R.; Grayson, B.; Fanson, P. and Datye, A. K., The definition of "critical radius" for a collection of nanoparticles undergoing Ostwald ripening, *Langmuir.* **2009**, 25, 11225–11227.
3. Dagtepe, P. and Chikan, V., Quantized Ostwald ripening of colloidal nanoparticles, *J. Phys. Chem. C.* **2010**, 114, 16263–16269.
4. Bai, Y.; Ye, L.; Chen, T.; Wang, L.; Shi, X.; Zhang, X. and Chen, D., Facet-dependent photocatalytic N_2 fixation of bismuth-rich Bi_5O_7I nanosheets, *ACS Appl. Mater. Interfaces,* **2016**, 8, 27661–27668.
5. Chen, Y.; Wang, F.; Cao, Y. H.; Zhang, F. Y.; Zou, Y. Z.; Huang, Z. A.; Ye, L. Q. and Zhou, Y., Interfacial oxygen vacancy engineered two-dimensional g-C_3N_4/BiOCl heterostructures with boosted photocatalytic conversion of CO_2, *ACS Appl. Energ. Mater.* **2020**, 3, 4610–4618.